# Large-amplitude and widely tunable self-oscillations enabled by the inertial effect in uniaxial antiferromagnets driven by spin-orbit torques

Peng-Bin He*
*School of Physics and Electronics, Hunan University, Changsha 410082, China*

(Received 24 July 2023; accepted 6 November 2023; published 20 November 2023)

Recently, the inertia has been demonstrated for magnetization dynamics, such as the nutational resonance and spin wave, as well as the inertial switching. Here, we focus on the inertial effect of self-oscillations induced by the spin-orbit torques in easy-axis antiferromagnets. Utilizing the stability analysis of equilibria and the exact solution of precession, we analytically construct the phase diagram controlled by the current and the inertial relaxation time. We then show that the magnetic inertia expands the tunable range of oscillation, the frequency of which is in the terahertz regime. Meanwhile, the frequency is proportional to the current and can enter an ultrahigh regime. Particularly, a lager-amplitude oscillation always persists when increasing the current. These features stand in sharp contrast to the case without an inertia, for which the amplitude of oscillation decreases with an increasing current and the oscillation fades away beyond a critical current. Our results not only enrich the nonlinear magnetic dynamics involving the inertial effect but also provide guidelines for the terahertz application of antiferromagnetic spintronics.

DOI: 10.1103/PhysRevB.108.184418

## I. INTRODUCTION

Terahertz (THz) oscillations have raised a great interest for multifarious applications, such as biomedical imaging, industrial product inspection, security check, and wireless communication [1]. Magnetization oscillations in antiferromagnets (AFMs) have the potential to realize the emitting and receiving of THz signals. Due to the exchange enhancement, the frequencies, of both the linear and nonlinear AFM oscillations, fall into the THz range. Furthermore, they can be manipulated by spin-orbit torques (SOTs) [2], which are generally produced in a simple bilayer structure consisting of a current-driven heavy-metal layer and an AFM one. Mathematically, SOTs can be decomposed into two perpendicular components: the fieldlike SOT (FLSOT) and the dampinglike SOT (DLSOT). The former acts as an effective field proportional to the current. The latter can pump energy into or dissipate energy from the system, depending on the current polarity. So, increasing attentions have been attracted on the THz oscillations, especially driven by the SOTs, in the synthetic [3–8], collinear [9–23], canted [24], and noncollinear trisublattice AFMs [25–29], as well as the ferrimagnets [30–32].

Although these investigations may contribute to the understanding of the AFM oscillator from viewpoints of both fundamental and applied physics, we note that there exists a question bringing about a disadvantage for application. Generally, the oscillating frequency, which is almost proportional to the strength of SOTs in most previous studies, can be adjusted by the current. However, when increasing the current, the precessional angle decreases in order to keep the balance between the DLSOT and the damping. Correspondingly, the amplitude of oscillation is getting smaller and smaller, so that the oscillation disappears with the current beyond a critical value. This leads to a finite tunable range of the oscillating frequency and a weak power output. There are several attempts to remove this shortcoming. For instance, Khymyn *et al.* [11] introduced a sufficiently strong easy-plane anisotropy, compelling the magnetic moments to precess in plane, and then maintaining a large-amplitude oscillation. Zhao *et al.* [23] confirmed that the tunable range can be optimized by changing the anisotropy or the damping.

Here, inspired by recent studies on magnetic inertial effects [33], we want to explore how the magnetic inertia influences the THz nonlinear oscillation, and overcomes the shortcoming mentioned above. Phenomenologically, magnetic inertia emerges as a term including a second time derivative of the magnetization in the Landau-Lifshitz-Gilbert (LLG) equation. It was argued that the magnetic inertia arises from an instantaneous noncollinearity between the magnetization and the angular momentum. Inspired by a hint of inertial effect mentioned by Gilbert in deriving the damping term [34], the inertial term in the LLG equation has been derived in the framework of mesoscopic nonequilibrium thermodynamics theory [35], obtained by a mechanical analogy of the magnetic moment with the spinning top [36], and derived from the classical mechanics of a circular current loop [37]. In addition, it can also be derived by series expansions of some integrodifferential equations on the basis of the extended breathing Fermi surface model [38,39], the Dirac theory [40,41], the retardation effect [42], the s-d interaction [43], and the interaction between a magnetic moment and a vector bath [44]. The typical inertial effect is the nutation, which has been observed indirectly [45]. Subsequently, direct evidence was presented [46,47] as technologies, e.g., the high-frequency magnetic field, developed. Besides, there were a boom of theoretical studies on the inertial effects, including the nutation

*hepengbin@hnu.edu.cn

 

resonances in ferromagnets [48–55] and AFMs [56–58], the nutation spin waves [59–63], and the nutational switching [64–67].

For dc-current-driven spin-valve or spin Hall heterostructures, when the dampinglike spin-transfer torque or the DLSOT compensates the intrinsic magnetic damping, a magnetic self-oscillation may be triggered, which generates self-sustained ac signals from dc inputs. For ferromagnetic systems, this oscillation, with the frequency in the GHz regime, is propelled by the external magnetic field, the anisotropy field, or the demagnetization field [68,69]. By contrast, in antiferromagnetic or ferrimagnetic systems, the self-oscillation is mainly driven by the strong exchange interactions, leading to THz frequencies [10,11,22,23,28,31]. In particular, the AFM self-oscillations, which occur in a simple setup and can be operated in the absence of external magnetic fields, make it possible to realize compact nanosized electrical generators and receivers of THz signals. So far, the effect of magnetic inertia on the self-oscillation of magnetization is unexplored. Therefore, in this paper, we will study the influence of magnetic inertia on the self-oscillations in the uniaxial AFMs driven by the SOTs.

The present work is organized as follows. After introduction Sec. I and model description Sec. II, we present the attenuation and dispersion of precessional and nutational linear modes for small currents and derive the instability condition by linear stability analysis, see Sec. III supplemented with Appendix B. Section IV and Appendix C are devoted to the magnetic phase diagram and the detailed analysis of self-oscillations triggered by the SOTs in the presence of magnetic inertia. We finally discuss and summarize our results in Secs. V and VI.

## II. MODEL

The considered model is a layered structure consisting of a current-driven heavy-metal (HM) layer and a layer of the AFM with an easy-axis anisotropy. Including the current-induced SOTs [2] and the inertial effect, the AFM dynamics is ruled by two coupled LLG equations,

$$\dot{\mathbf{m}}_i = \mathbf{m}_i \times \frac{\partial E}{\partial \mathbf{m}_i} + \alpha \mathbf{m}_i \times \dot{\mathbf{m}}_i + \eta \mathbf{m}_i \times \ddot{\mathbf{m}}_i + \tau_i, \qquad (1)$$

where $\mathbf{m}_i$ stands for a unit vector along the magnetization of the $i$th sublattice with $i = 1, 2$, and the overdot denotes time derivation. All the terms in Eq. (1) have been rescaled to have the dimension of frequency.

The first term on the right-hand side of Eq. (1) represents the precession propelled by the effective internal fields due to the exchange interaction and the magnetocrystalline anisotropy. The magnetic energy in this term reads

$$E = \omega_E \mathbf{m}_1 \cdot \mathbf{m}_2 - \omega_K \sum_{i=1}^{2} (\mathbf{m}_i \cdot \mathbf{e}_z)^2, \qquad (2)$$

where $\omega_E = \gamma_0 H_E$, and $\omega_K = \gamma_0 H_K$, with $H_E$ being the effective field due to the intersublattice exchange coupling, and $H_K$ the anisotropy field. $\gamma_0 = g\mu_0\mu_B/\hbar$ is the gyromagnetic ratio with $g$ being the Landé $g$ factor, $\mu_0$ the vacuum susceptibility, $\mu_B$ the Bohr magneton, and $\hbar$ the reduced Plank constant.

The second term is the damping torque with $\alpha$ being Gilbert constant. The third term, involving the second time derivative of the magnetization vectors, is a torque from the magnetic inertia. $\eta$ is the inertial relaxation time ranging from fs to ps, as predicted in the *ab initio* calculation [70] and the nutation experiments [45–47].

The fourth term is the SOTs expressed as

$$\tau_i = -\omega_T \mathbf{m}_i \times (\mathbf{m}_i \times \mathbf{e}_z) - \beta\omega_T (\mathbf{m}_i \times \mathbf{e}_z), \qquad (3)$$

with the spin polarization along the $z$ axis and $\beta$ denoting the ratio of the FLSOT to the DLSOT. In the unit of frequency, the strength of SOTs reads

$$\omega_T = \frac{\mu_B}{eM_s d}\xi j_e, \qquad (4)$$

with $d$ being the thickness of the AFM layer, $e$ the element charge, $M_s$ the sublattice saturation magnetization, and $j_e$ the electric current density. $\xi$ is the SOT efficiency, which equals to $T_{\rm int}\theta_{sh}$ [71,72], with $\theta_{sh}$ being the spin Hall angle, and $T_{\rm int}$ the spin transparency of the interface [73].

## III. LINEAR OSCILLATIONS

Without the SOTs, the system is in two equivalent AFM states ($\mathbf{m}_1^0 = \pm\mathbf{e}_z$ and $\mathbf{m}_2^0 = \mp\mathbf{e}_z$). For small currents, linear modes are excited around an AFM configuration, which can be represented by an oscillating ansatz,

$$\mathbf{m}_i = (-1)^{i-1}\mathbf{e}_z + X_i e^{\lambda t}\mathbf{e}_x + Y_i e^{\lambda t}\mathbf{e}_y. \qquad (5)$$

Here $X_i$ and $Y_i$, which are assumed as small quantities, are the amplitudes of oscillating modes. The oscillating feature is represented by a complex factor,

$$\lambda = -\chi + i\omega, \qquad (6)$$

with $\chi$ being the attenuation factor and $\omega$ the oscillating frequency. Inserting Eq. (5) into Eq. (1), and truncating the LLG equations at the linear order of $X_i$ and $Y_i$, we get the linearized equation in the vicinity of an AFM state,

$$\begin{pmatrix} \lambda+\omega_T & f^+(\lambda) & 0 & \omega_E \\ -f^+(\lambda) & \lambda+\omega_T & -\omega_E & 0 \\ 0 & -\omega_E & \lambda-\omega_T & -f^-(\lambda) \\ \omega_E & 0 & f^-(\lambda) & \lambda-\omega_T \end{pmatrix} \begin{pmatrix} X_1 \\ Y_1 \\ X_2 \\ Y_2 \end{pmatrix} = 0, \qquad (7)$$

where $f^{\pm}(\lambda) = \eta\lambda^2 + \alpha\lambda + \omega_E + 2\omega_K \pm \beta\omega_T$. Note that Eq. (7) is identical for two AFM states. To ensure the solution of Eq. (7) nontrivial, the determinant of coefficient matrix must be zero, leading to a secular equation,

$$\sum_{i=0}^{8} a_i \lambda^{8-i} = 0, \qquad (8)$$

where $a_0 = \eta^4$, $a_1 = 4\alpha\eta^3$, $a_2 = 2[1 + 3\alpha^2 + 2\eta(\omega_E + 2\omega_K)]\eta^2$, $a_3 = 4\alpha[1 + \alpha^2 + 3\eta(\omega_E + 2\omega_K)]\eta$, $a_4 = (1 + \alpha^2)^2 + 4(\omega_E + 2\omega_K)(1 + 3\alpha^2)\eta + 2[2(\omega_E^2 + 6\omega_E\omega_K + 6\omega_K^2) + (1 - \beta^2)\omega_T^2]\eta^2$, $a_5 = 4\alpha(1 + \alpha^2)(\omega_E + 2\omega_K) + 4\{2\alpha(\omega_E^2 + 6\omega_E\omega_K + 6\omega_K^2) + [(\alpha - \beta) - (1 + \alpha\beta)\beta]\omega_T^2\}\eta$, $a_6 = 8\omega_K$

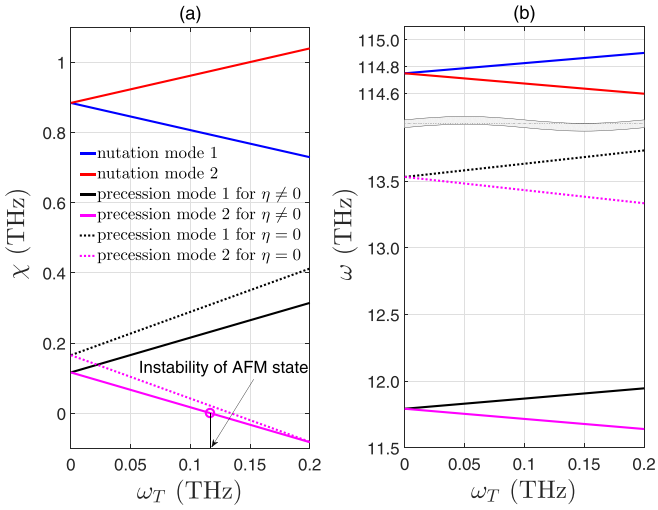


FIG. 1. (a) The attenuation $\chi$ and (b) the frequency $\omega$ of the linear oscillation based on the AFM configuration. The dotted and solid lines correspond to the case that $\eta = 0$ and $\eta \neq 0$, respectively. The values of the magnetic parameters are brought from $FeF_2$ [74,75]. The exchange field $H_E = 540$ kOe and the anisotropy field $H_K = 200$ KOe, corresponding to $\omega_E = 9.5$ THz and $\omega_K = 3.5$ THz. The other parameters are $\alpha = 0.01$, $\beta = 1$, and $\eta = 10$ fs.

$(\omega_E + \omega_K) + 4\alpha^2(\omega_E^2 + 6\omega_E\omega_K + 6\omega_K^2) - 2[(1+\alpha\beta)^2 - (\alpha - \beta)^2]\omega_T^2 + 4(\omega_E + 2\omega_K)[4\omega_K(\omega_E + \omega_K) + (1-\beta^2)\omega_T^2]$ $\eta$, $a_7 = 4(\omega_E + 2\omega_K)\{4\alpha\omega_K(\omega_E + \omega_K) + [(\alpha - \beta) - (1 + \alpha\beta)\beta]\omega_T^2\}$, $a_8 = [(1+\beta^2)\omega_T^2 - 4\omega_K(\omega_E + \omega_K)]^2 + 4(\omega_E + 2\omega_K)^2\omega_T^2$. This is an eighth-order algebraic equation with the high-order terms arising from the magnetic inertia. Note that $a_0$, $a_1$, $a_2$, and $a_3$, which are of higher order in $\lambda$, are proportional to $\eta$. Setting $\eta = 0$, Eq. (8) turns into a fourth-order equation.

In general, for the $n$th-degree polynomial equations with real coefficients, the nonreal roots come in complex conjugate pairs. So, the modes with negative frequencies have the same attenuation factors as their positive counterparts. We then solve Eq. (8) numerically and only show the dispersion for positive frequency in Fig. 1(b), and the dependence of the attenuation factor on the strength of SOTs in Fig. 1(a).

Several conclusions can be made from Eqs. (5)–(8) and Fig. 1. (i) The presence of inertia leads to a red shift of the precessional modes, illustrated by comparing the solid lines and the dotted ones in the bottom panel of Fig. 1(b). (ii) The nutation modes appear if involving the inertial term, as shown by solid lines in the top panel of Fig. 1(b). (iii) The SOTs break the degeneracy of both the precession and nutation modes, and the frequency gap grows with the current (i.e., $\omega_T$) increasing. (iv) Along with $\omega_T$ increasing, the attenuation factor of one mode becomes zero first, as marked by the circle point in Fig. 1(a). Beyond this point, the AFM state is unstable. By the linear stability analysis and the Routh-Hurwitz criterion [76–78], it can be inferred that the AFM state turns unstable if $|\omega_T| > \omega_T^a$, which reads (see Appendix A for details of the derivation),

$$\omega_T^a = \frac{\alpha}{\sqrt{2}\eta}\sqrt{(1+\alpha\beta)^2 + 2\eta(\omega_E + 2\omega_K) - \sqrt{\left[(1+\alpha\beta)^2 + 2\eta(\omega_E + 2\omega_K)\right]^2 - 16\eta^2\omega_K(\omega_E + \omega_K)}}. \tag{9}$$

It can be checked that $\omega_T^a$ decreases with $\eta$ increasing. This indicates that the switching from an AFM state to the self-oscillation is easy for strong magnetic inertia. Especially, expanding to lowest nonvanishing order in $\eta$, we get $\omega_T^a = (2\alpha)/(1+\alpha\beta)\sqrt{\omega_K(\omega_E + \omega_K)}[1 - 1/(1+\alpha\beta)^2(\omega_E + 2\omega_K)\eta]$. In the limit of $\eta \to 0$, the value of $\omega_T^a$ is consistent with the result without inertia [22].

## IV. SELF-OSCILLATIONS

### A. Precession solution and phase diagram

After the breakdown of the linear modes based on an AFM configuration, the system may enter other equilibria or dynamic states, especially, the large-amplitude self-oscillation, which is determined by the nonlinear characteristics of the system. In view of the rotational symmetry around the $z$ axis, the system allows $m_{1x} = -m_{2x}$, $m_{1y} = -m_{2y}$, and $m_{1z} = m_{2z}$. Then, a precessional solution can be derived analytically, which reads,

$$m_{1x} = -m_{2x} = \sqrt{1 - m_{1z}^2}\cos(2\pi f t + \varphi_0), \tag{10}$$

$$m_{1y} = -m_{2y} = \sqrt{1 - m_{1z}^2}\sin(2\pi f t + \varphi_0), \tag{11}$$

$$m_{1z} = m_{2z} = \frac{\alpha(1+\alpha\beta)\omega_T}{2\alpha^2(\omega_E - \omega_K) + \eta\omega_T^2} \tag{12}$$

with $\varphi_0$ being the initial phase. The frequency

$$f = -\frac{1}{2\pi}\frac{\omega_T}{\alpha}. \tag{13}$$

For this solution, $\mathbf{m}_1$ and $\mathbf{m}_2$ precess around the $z$ axis and keep antiphase. The minus in Eq. (13) means that the rotation around the positive $z$ direction is left handed (right handed) for positive (negative) $\omega_T$. To ensure the existence of this solution, $|m_{1z}| = |m_{2z}| < 1$. Namely, $(|\omega_T| - \omega_{T+}^c)(|\omega_T| - \omega_{T-}^c) > 0$, where

$$\omega_{T\pm}^c = \frac{\alpha}{2\eta}(1+\alpha\beta)\left(1 \pm \sqrt{1 - \frac{\eta}{\eta_c}}\right), \tag{14}$$

with

$$\eta_c = \frac{(1+\alpha\beta)^2}{8(\omega_E - \omega_K)}. \tag{15}$$

In view of the strong exchange interaction, it is reasonable to assume that $\omega_E > \omega_K$. Then, solving this inequation for $\eta < \eta_c$, we have $|\omega_T| < \omega_{T-}^c$ or $|\omega_T| > \omega_{T+}^c$. As derived in Appendix B, $\omega_{T\pm}^c$ also defines the instability lines of

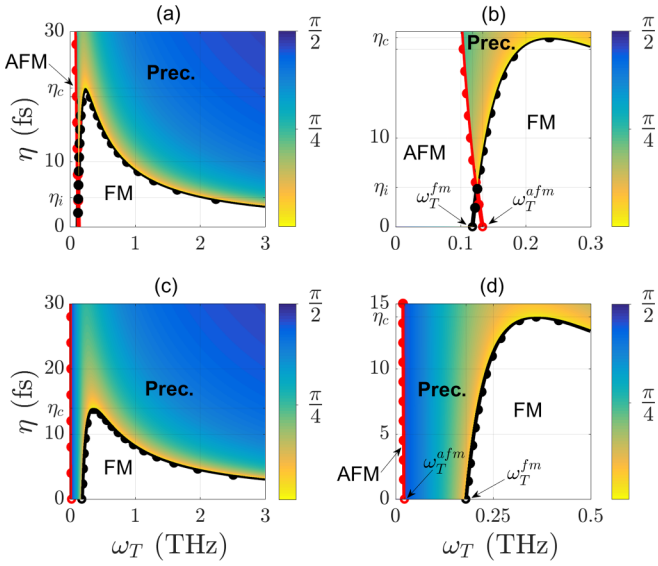


FIG. 2. Phase diagrams in the parameter plane spanned by the SOT strength $\omega_T$ and the inertial relaxation time $\eta$. (b) and (d) are closer views of (a) and (c), respectively, in the region with small $\omega_T$. The red lines represent $\omega_T^a$ [Eq. (9)]. The black curves represent $\omega_{T\pm}^c$ [Eq. (14)]. The filled circles are plotted by numerically integrating Eq. (1). The red and black circle points correspond to $\omega_T^a$ and $\omega_{T-}^c$ at $\eta = 0$. In the colored regions, the self-oscillation (marked by Prec.) exists. The color scale indicates the precessional angle $\theta$. In (a) and (b), we use the magnetic parameters of $FeF_2$ [74,75]. The exchange field $H_E = 540$ kOe and the anisotropy field $H_K = 200$ kOe, corresponding to $\omega_E = 9.5$ THz and $\omega_K = 3.5$ THz. In (c) and (d), we use those of $MnFe_2$ [74,79]. $H_E = 526$ kOe and $H_K = 8.2$ kOe, corresponding to $\omega_E = 9.25$ THz and $\omega_K = 0.14$ THz. The other parameters are $\alpha = 0.01$, and $\beta = 1$.

the FM states. When $\omega_{T-}^c \leqslant |\omega_T| \leqslant \omega_{T+}^c$, $|m_{1z}| = |m_{2z}| \geqslant 1$ and the precessional state is unstable. As demonstrated in Appendix B, the FM state with $\mathbf{m}_1^0 = \mathbf{m}_2^0 = \mathbf{e}_z$ is stable for $\omega_{T-}^c \leqslant \omega_T \leqslant \omega_{T+}^c$, and the other FM state with $\mathbf{m}_1^0 = \mathbf{m}_2^0 = -\mathbf{e}_z$ is stable for $-\omega_{T+}^c \leqslant \omega_T \leqslant -\omega_{T-}^c$. If $\eta > \eta_c$, $\omega_{T\pm}^c$ are conjugate complex. From Eq. (12), it is easy to infer that, $|m_{1z}| = |m_{2z}| < 1$ for arbitrary $\omega_T$. This means that the precession always exists for $|\omega_T| > \omega_T^a$.

Based on Eqs. (9) and (14), we build the phase diagrams controlled by $\omega_T$ and $\eta$ in Fig. 2 for the AFMs with a strong or weak anisotropy. According to the stability analysis of AFM (see Appendix B) and FM states (see Appendix C), we find that there is no stable equilibrium state in some parameter regions, which are colored areas in Fig. 2. By integrating Eq. (1) numerically, the evolution of magnetization indicates that self-oscillations arise when $\omega_T$ and $\eta$ locate in these areas.

One direct observation form Fig. 2 is that when $\eta > \eta_c$, the self-oscillation always occurs for $\omega_T > \omega_T^a$. If $\eta < \eta_c$, two cases need to be distinguished, depending on the relative magnitude of the anisotropy to the exchange interaction. If $\omega_K > \omega_E/3$, $\omega_T^a > \omega_{T-}^c$ for $\eta < \eta_i$, with

$$\eta_i = 3(1+\alpha\beta)^2 \frac{3\omega_K - \omega_E}{8\omega_E^2}. \tag{16}$$

$\eta_i$ is obtained by solving $\omega_T^a = \omega_{T-}^c$ and is labeled in Figs. 2(a) and 2(b). It can be concluded that, for any $\omega_T$ between $\omega_T^a$ and $\omega_{T-}^c$, only the FM or AFM exists and there does no self-oscillation happen if $\eta < \eta_i$, as shown in Figs. 2(a) and 2(b). Specially, in the absence of inertial term, no self-oscillation occurs in this case. At $\eta = 0$, from Eqs. (9) and (14), we get the critical values of $\omega_T$ for AFM and FM states,

$$\omega_T^{afm} = \frac{2\alpha}{1+\alpha\beta}\sqrt{\omega_K(\omega_E+\omega_K)}, \tag{17}$$

$$\omega_T^{fm} = \frac{2\alpha}{1+\alpha\beta}(\omega_E - \omega_K). \tag{18}$$

These two values are marked by the open dots in Fig. 2(b). In general, when $\omega_T < \omega_T^{afm}$, the AFM state is stable. And when $\omega_T > \omega_T^{fm}$, the FM state is stable. Here, $\omega_T^{fm} < \omega_T^{afm}$ if $\omega_K > \omega_E/3$ (for example, the uniaxial AFM $FeF_2$), resulting in a bistable state of FM and AFM, and then excluding the self-oscillation in this interval from $\omega_T^{fm}$ to $\omega_T^{afm}$, as displayed in Fig. 2(b).

By contrast, when $\omega_K < \omega_E/3$ (for example, the uniaxial AFM $MnF_2$), $\omega_T^{fm} > \omega_T^{afm}$. Thus, in the interval from $\omega_T^{afm}$ to $\omega_T^{fm}$, both AFM and FM equilibria are unstable and the self-oscillation exists, as displayed in Figs. 2(c) and 2(d).

### B. Analogy with spin flop and spin flip

As regards above-mentioned difference between the weak anisotropy and the strong one, it is interesting to take an analogy with the spin-flop and spin-flip transitions of AFM under an magnetic field [80,81]. Both of the transitions are triggered by an increasing magnetic field along the easy axis of AFM. The spin flop occurs for a weak anisotropy. At a critical field, the system suddenly snaps from an antiparallel state into a configuration with $\mathbf{m}_1$ and $\mathbf{m}_2$ at a same angle with respect to the easy axis. This is similar to the case of $\omega_K < \omega_E/3$, for which the angle between $\mathbf{m}_1$ and the easy axis is equal to that between $\mathbf{m}_2$ and the easy axis. But, unlike the static spin-flop state, for which no external torques can cancel the damping, in this case $\mathbf{m}_{1,2}$ precesses steadily around the easy axis when the Gilbert damping is compensated by the DLSOT. On the other hand, if $\omega_K > \omega_E/3$, the SOTs flip $\mathbf{m}_1$ ($\mathbf{m}_2$) to $\mathbf{m}_2$ ($\mathbf{m}_1$) at the critical $\omega_T$, similar to the field-triggered spin-flip transition for a strong anisotropy.

### C. Tunability of self-oscillation

From the precession solution and the phase diagram, we can conclude that the presence of inertia extends the range of $\omega_T$ for the self-oscillation. For a relatively strong anisotropy, as shown in Figs. 2(a) and 2(b), there does no precession appear for any $\omega_T$ if $\eta = 0$. When $0 < \eta < \eta_i$, the system turns from the AFM state to the FM one with an increasing $\omega_T$ across $\omega_T^a$. If increasing $\omega_T$ further, the self-oscillation happens beyond $\omega_T^{c+}$. When $\eta_i < \eta < \eta_c$, the system switches from the AFM state to the precession at $\omega_T^a$, and then enter the FM state with $\omega_T$ crossing $\omega_T^{c-}$. With $\omega_T$ increasing further, the self-oscillation revives when $\omega_T > \omega_T^{c+}$. When $\eta > \eta_c$, the self-oscillation always exists if $\omega_T > \omega_T^a$. The case is different for a relative weak anisotropy, for which the self-oscillation exists for any $\eta$. As shown in Figs. 2(c) and 2(d), if $0 \leqslant \eta <$

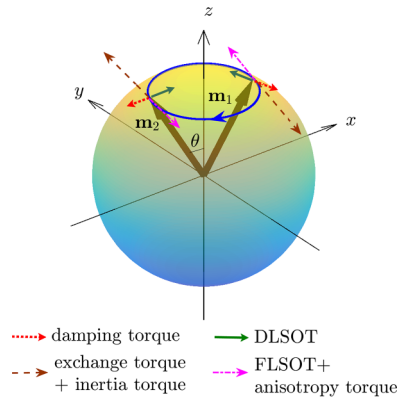


FIG. 3. A sketch of all the torques exerted on $\mathbf{m}_1$ and $\mathbf{m}_2$. Here, the precession is triggered by a position $\omega_T$ and the orbit is on the hemisphere of $m_{1z,2z} > 0$.

$\eta_c$, the AFM state, the precession, the FM state, and another precession appear in turn when increasing $\omega_T$. If $\eta > \eta_c$, the case is the same as the strong anisotropy. With $\eta$ increasing, the range of precession widens for both cases. Given that the frequency is proportional to $\omega_T$ [Eq. (13)], the extension of the $\omega_T$ range also broadens the frequency range, further enabling an ultrahigh frequency.

Moreover, to understand the extension of precession range due to the inertia, it is instructive to take an intuitive argument based on the vector analysis of all the torques exerted on $\mathbf{m}_{1,2}$, as schematically shown in Fig. 3. For the considered system, there are six kinds of torques in total. The intrinsic damping toque $[\alpha\mathbf{m}_{1(2)} \times d\mathbf{m}_{1(2)}/dt]$ points along the normal of precessional cone. For a right-handed rotation, it points towards the precessional axis ($z$ axis) and decreases the precessional angle. While, for a left-handed rotation (the case displayed in Fig. 3), the damping torque turns $\mathbf{m}_{1,2}$ away from the rotation axis. The DLSOT $[-\omega_T\mathbf{m}_{1(2)} \times (\mathbf{m}_{1(2)} \times \mathbf{e}_z)]$ is also along the normal of precessional cone, and in our sign convention, directs to the $z$ axis for positive $\omega_T$. Both the damping torque and the DLSOT are on the same line. To realize a self-oscillation, the DLSOT must cancel the damping. If their directions are identical, the self-oscillation cannot happen. If they are opposite, a self-oscillation possibly occurs. So, as shown in Fig. 3, under the SOTs with positive $\omega_T$, only the left-handed precession possibly exists owing to the balance between the damping and the DLSOT.

The other four torques are along the tangential of precessional cone, as indicated in Fig. 3. By use of Eqs. (10)–(12), the exchange torque $[\omega_E\mathbf{m}_{1(2)} \times \mathbf{m}_{2(1)}]$ born by $\mathbf{m}_{1(2)}$ can be expressed as $\omega_E \cos\theta\mathbf{m}_{1(2)} \times \mathbf{e}_z$ with $\theta$ being the precessional angle. This torque propels $\mathbf{m}_{1,2}$ rotating left handedly. Also, from Eqs. (10)–(12), the inertia torque $\eta\mathbf{m}_{1(2)} \times \ddot{\mathbf{m}}_{1(2)}$ is written as $\eta\omega^2 \cos\theta\mathbf{m}_{1(2)} \times \mathbf{e}_z$ with $\omega = 2\pi f$, which still results in a left-handed precession. This is in contrast to the precession in a ferromagnet, for which the inertial torque opposes and reduces the precessional torque produced by the anisotropy or the magnetic field [54].

The anisotropy torque and the FLSOT enable a right-handed precession. The sum of them reads $-(\omega_K \cos\theta + \beta\omega_T)\mathbf{m}_{1(2)} \times \mathbf{e}_z$. Considering the strong AFM exchange coupling and consequent high frequency, the exchange and inertial torques generally overwhelm the anisotropy torque and the FLSOT. Therefore, $\mathbf{m}_1$ and $\mathbf{m}_2$ rotate left handedly.

In the absence of inertia ($\eta = 0$), the precession is mainly driven by the exchange torque on the promise of a balance between the DLSOT and the damping. By Eq. (13), the frequency increases with $\omega_T$ increasing. This means that the exchange torque must increase. From the expression of exchange torque $[\omega_E \cos\theta\mathbf{m}_{1(2)} \times \mathbf{e}_z]$, the precessional angle $\theta$, which can serve as a measure of the oscillating amplitude (proportional to $\sin\theta$), becomes more and more smaller, until it vanishes. Thus, the region of self-oscillation is limited, as demonstrated in several previous works [17,22,23,28,32].

In the presence of inertia ($\eta \neq 0$), the dominant driving torques are $(\omega_E + \eta\omega^2)\cos\theta\mathbf{m}_{1(2)} \times \mathbf{e}_z$. The second term follows a parabolical dependence on $\omega$ and becomes significant for a high frequency. In experiment, it has been found that this term manifests itself in an additional stiffening of the ferromagnetic resonance [45]. If increasing $\omega_T$, the enhance of $\omega$ strengthens the driven torques, postponing the decrease of $\theta$ and enlarging the range of precession. Furthermore, when $\eta > \eta_c$, the term $\eta\omega^2$ is predominant. Even if $\theta$ increases ($\cos\theta$ decreases), the total driven torques still get stronger. Therefore, the self-oscillation always exists when increasing $\omega_T$. Above argument is displayed by the variation of the color scale in Fig. 2, which denotes the precessional angle $\theta$. Specially, for the stronger SOTs, $\theta$ is very close to $\pi/2$. Namely, the precession is almost in the $x$-$y$ plane.

### D. Effects of the fieldlike SOT

The FLSOT acts as a precessional torque like an external magnetic field. Recent experiments report that the FLSOT can be adjusted (examples of the literature are Refs. [82,83]), and even becomes much stronger than the DLSOT [82], as well as switches its sign [83]. First of all, we have checked the maps of the signs of Hurwitz determinants for different $\beta$ and find that $\omega_T^a$ of Eq. (9) is always the instability threshold of AFM state. For definiteness, we restrict above discussions to the case $1 + \alpha\beta > 0$ and positive $\omega_T$. If $1 + \alpha\beta < 0$, $m_{1z} = m_{2z} < 0$ for $\omega_T > 0$, and a similar analysis indicates that $\mathbf{m}_{1,2}$ rotates around $-\mathbf{e}_z$ left handedly.

It is interesting to consider a special scenario $1 + \alpha\beta = 0$, which, however, is not easily obtained by tuning the parameters at present. In this case, $\eta_c = 0$ [see Eq. (15)], $\omega_T^a = \sqrt{2}\alpha\sqrt{\omega_K/\eta}$ [see Eq. (9)]. Along with $\eta$ increasing, the system enter the self-oscillation state more easier. In addition, $\omega_{T\pm}^c = \pm i\sqrt{2}\alpha\sqrt{(\omega_E - \omega_K)/\eta}$ [obtained by taking the limit $1 + \alpha\beta \to 0$ in Eq. (14) or Eq. (C24)]. According to the stability analysis of FM state in Appendix C, complex $\omega_{T\pm}^c$ mean that the FM state can not emerge and the system always keeps the self-oscillation state beyond the instability of AFM state. Moreover, $m_{1z} = m_{2z} = 0$ [see Eq. (12)] for the oscillating solution, suggesting an exact in-plane precession. Also, these features can be understood by a simple argument based on the vector calculation. According to the LLG equations [Eqs. (1)–(3)] and the precessional solution Eqs. (10)–(13) for the case $1 + \alpha\beta = 0$, the precessional torques from the exchange interaction, the anisotropy, and the inertia vanish for this in-plane precession ($\mathbf{m}_i \times \frac{\partial E}{\partial \mathbf{m}_i} = 0$, and $\eta\mathbf{m}_i \times \ddot{\mathbf{m}}_i = 0$). The damping torque $\alpha\mathbf{m}_i \times \frac{d\mathbf{m}_i}{dt} = -\omega_T\mathbf{e}_z$, which is offset by the

DLSOT $[(-\omega_T \mathbf{m}_i \times (\mathbf{m}_i \times \mathbf{e}_z) = \omega_T \mathbf{e}_z]$. Both of them are proportional to $\omega_T$. So, the balance always holds for any $\omega_T$ and the FM state can not emerge when increasing $\omega_T$. Moreover, the precession is propelled only by the FLSOT $-\beta\omega_T \mathbf{m}_i \times \mathbf{e}_z$. For this in-plane precession, the rate of change of $\mathbf{m}_i$ can be expressed as $\dot{\mathbf{m}}_i = -2\pi f \mathbf{m}_i \times \mathbf{e}_z = \frac{\omega_T}{\alpha}\mathbf{m}_i \times \mathbf{e}_z$. Then, the condition $1 + \alpha\beta = 0$ is obtained consistently from $\dot{\mathbf{m}}_i = -\beta\omega_T \mathbf{m}_i \times \mathbf{e}_z$.

## V. DISCUSSION

Before ending this paper, several remarks are in order. First, in the above concise deduction, the strengths of various torques are scaled in unit of frequency, including that of SOTs. Here, from Eq. (4), we estimate the current density corresponding to relevant $\omega_T$. $\eta_c$ is an important parameter. When $\eta > \eta_c$, the range of self-oscillation is dramatically enlarged. Taking the parameters in Fig. 2, $\eta_c$ is about 21 fs for $FeF_2$, and 14 fs for $MnF_2$. Although there is no experiment on the AFM inertial effect, these values of $\eta$ seem reasonable, if referring to the inertial relaxation time in FMs ranging from fs to ps (see Ref. [33] and references therein). Corresponding to $\eta_c$, $\omega_T^a$, beyond which the self-oscillation appears, is about 0.1046 THz for $FeF_2$, and 0.0205 THz for $MnF_2$. Taking $d = 3$ nm, $\xi = 0.32$, as well as $M_s = 44.6$ kA/m for $FeF_2$ [75] and 47.7 kA/m for $MnF_2$ [79] in Eq. (4), the corresponding current densities are $7.55 \times 10^{11}$ A/m$^2$ and $1.59 \times 10^{11}$ A/m$^2$, respectively. These values are moderate in experiment. From Eq. (13), the lowest frequency of self-oscillation is 1.664 THz for for $FeF_2$, and 0.3267 THz for $MnF_2$. When increasing the current, this frequency increases unlimitedly for $\eta > \eta_c$ and is in the THz ranges.

Second, although the inertial effect is observed only in FMs at present, it seems to be naively believed that there also exists inertia in AFMs. It was demonstrated in an *ab initio* calculation that the magnetic inertia is produced by the spin-orbit coupling and can be tuned through the electronic structure [70]. So, some AFM materials with tunable inertia (different $\eta$) are expected.

Third, for the sake of completeness, we study both the linear and nonlinear oscillations of AFMs under the SOTs. The linear oscillations at small currents belong to the damped, small-amplitude, and resonancelike excitations, which can be used to detect the inertial relaxation time and the nutational frequency, for example, in the resonance experiment by applying an additional ac current. In comparison, the nonlinear oscillations is steady, self-sustained, and of large amplitude. Thus, it is preferable to use the self-oscillations to emit THz signals.

Finally, in this paper, we only investigate the case that the spin polarization of SOTs is parallel to the easy axis of AFMs, for which the analytic results can be obtained easily. For other magnetic configurations and SOT schemes, e.g., the AFMs with a biaxial anisotropy or the SOTs with an arbitrary spin polarization, the analytic calculations are very complicated. However, there is a similar qualitative physics. When increasing the current, the sublattice magnetization $\mathbf{m}_{1,2}$ rotate around the spin-polarization direction left handedly [10,11,16,22,23] after the instability of AFM ground state. According to the qualitative analysis in Sec. IV C, it can be argued that the inertial torque accelerates this precession and allows large-amplitude oscillations. But, a more detailed understanding of this phenomenon for other SOTs-driven AFMs with different configurations require a separate analysis, which is beyond the scope of this work and will be pursued in the future.

## VI. SUMMARY

In summary, we investigate the linear and nonlinear oscillations driven by the SOTs in uniaxial AFMs based on two coupled inertial LLG equations. For the linear oscillation, we find that the magnetic inertia results in a red shift of the precessional mode and the emergence of a high-frequency nutation mode. The SOTs lift the degeneracies of both the precession and the nutation. Moreover, the phase boundary of nonlinear oscillation (self-oscillation) is defined by the stability analysis of AFM and FM equilibria as well as the analytic precessional solution. From the phase diagram, it can be revealed that the region of self-oscillation is expanded in the presence of inertia. Especially, when the inertial relaxation time is greater than a critical value ($\eta > \eta_c$), the system will no longer enter the FM state and the self-oscillation always persists for arbitrary high currents. Additionally, the frequency is proportional to the current and can access the ultrahigh regime. When increasing the current, the precession almost keeps in-plane, ensuring a large-amplitude oscillation. For a special scenario that $1 + \alpha\beta = 0$, an exact in-plane precession appears as long as the AFM state becomes unstable. From an application perspective, these features of ultrahigh frequency and large amplitude, as well as the expanded tunable region of self-oscillation, provide an attractive and novel clue for the AFM THz technique.

## ACKNOWLEDGMENTS

This work was supported by the NSF of Changsha City (Grant No. kq2208008) and the NSF of Hunan Province (Grant No. 2023JJ30116).

## APPENDIX A: EQUILIBRIA

To study the linear and nonlinear oscillations, it is convenient to start from the equilibrium states under the SOTs, which are defined by the equilibrium between the precessional torque and the SOTs. Setting $\dot{\mathbf{m}}_i = 0$ in Eq. (1), these equilibria satisfy

$$\omega_E \mathbf{m}_i \times \mathbf{m}_{3-i} - \omega_K (\mathbf{m}_i \cdot \mathbf{e}_z)(\mathbf{m}_i \times \mathbf{e}_z) - \omega_T \mathbf{m}_i \times (\mathbf{m}_i \times \mathbf{e}_z) - \beta\omega_T (\mathbf{m}_i \times \mathbf{e}_z) = 0. \quad \text{(A1)}$$

In view of the rotation symmetry about the $z$ axis, it is easy to find that there are two kinds of equilibria. One is two equivalent AFM states, which is written as $\mathbf{m}_1^0 = \pm\mathbf{e}_z$ and $\mathbf{m}_2^0 = \mp\mathbf{e}_z$. The other is two opposite FM states $\mathbf{m}_1^0 = \mathbf{m}_2^0 = \pm\mathbf{e}_z$.

## APPENDIX B: STABILITY OF AFM STATES

Now, let us analyze the stability of AFM states first. According to the regular procedure of linear stability analysis,

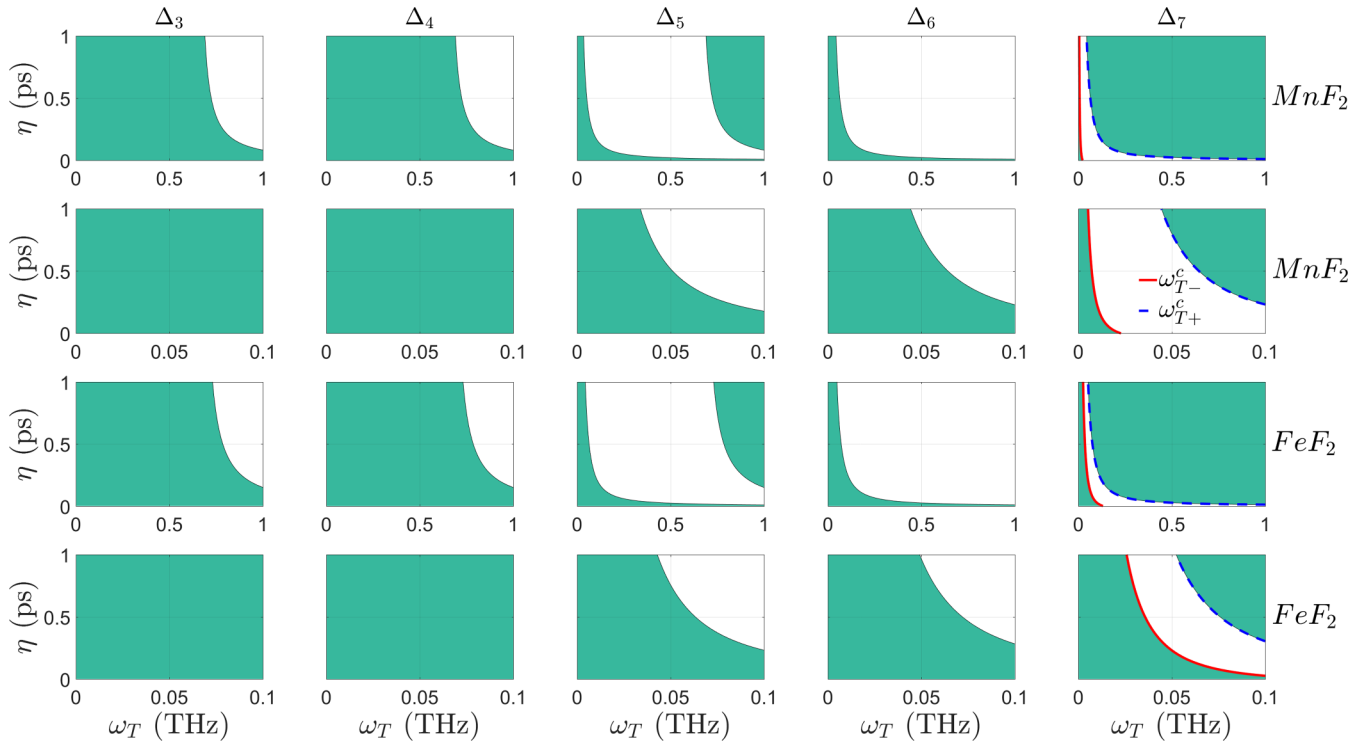


FIG. 4. Maps of the signs of Hurwitz determinants ($\Delta_{3-7}$) in the parameter plane spanned by the SOT strength $\omega_T$ and the inertial relaxation time $\eta$. The shaded areas cover the range of parameters for positive $\Delta_{3-7}$. For the panels in the first and second (third and fourth) rows, the magnetic parameters of $MnF_2$ ($FeF_2$) are used. The panels in the second and fourth rows show magnified views at small $\omega_T$. The columns from left to right correspond to $\Delta_3$, $\Delta_4$, $\Delta_5$, $\Delta_6$, and $\Delta_7$ in turn. Here, $\alpha = 0.01$ and $\beta = 1$. The magnetic parameters of $FeF_2$ [74,75] are $H_E = 540$ kOe and $H_K = 200$ kOe, corresponding to $\omega_E = 9.5$ THz and $\omega_K = 3.5$ THz. Those of $MnFe_2$ [74,79] are $H_E = 526$ kOe and $H_K = 8.2$ kOe, corresponding to $\omega_E = 9.25$ THz and $\omega_K = 0.14$ THz.

we will linearize Eq. (1) in the vicinity of the AFM equilibria. So, we obtain the secular equation [Eq. (8)] of the linear oscillating ansatz Eq. (5). Based on this secular equation, we analyze the dispersion and attenuation of the linear modes in Sec. III of the main text. Here, by use of the Routh-Hurwitz criterion [76–78], we attempt to obtain the analytic expression of the instability condition of AFM states. It is argued that, if all the roots of Eq. (8) have a negative real part, the corresponding equilibrium state is stable. Then, we define a series of determinants,

$$\Delta_1 = a_1, \tag{B1}$$

$$\Delta_2 = \begin{vmatrix} a_1 & a_0 \\ a_3 & a_2 \end{vmatrix}, \tag{B2}$$

$$\Delta_3 = \begin{vmatrix} a_1 & a_0 & 0 \\ a_3 & a_2 & a_1 \\ 0 & a_4 & a_3 \end{vmatrix}, \tag{B3}$$

$$\Delta_4 = \begin{vmatrix} a_1 & a_0 & 0 & 0 \\ a_3 & a_2 & a_1 & a_0 \\ a_5 & a_4 & a_3 & a_2 \\ a_7 & a_6 & a_5 & a_4 \end{vmatrix}, \tag{B4}$$

$$\Delta_5 = \begin{vmatrix} a_1 & a_0 & 0 & 0 & 0 \\ a_3 & a_2 & a_1 & a_0 & 0 \\ a_5 & a_4 & a_3 & a_2 & a_1 \\ a_7 & a_6 & a_5 & a_4 & a_3 \\ 0 & a_8 & a_7 & a_6 & a_5 \end{vmatrix}, \tag{B5}$$

$$\Delta_6 = \begin{vmatrix} a_1 & a_0 & 0 & 0 & 0 & 0 \\ a_3 & a_2 & a_1 & a_0 & 0 & 0 \\ a_5 & a_4 & a_3 & a_2 & a_1 & a_0 \\ a_7 & a_6 & a_5 & a_4 & a_3 & a_2 \\ 0 & a_8 & a_6 & a_7 & a_5 & a_4 \\ 0 & 0 & 0 & a_8 & a_7 & a_6 \end{vmatrix}, \tag{B6}$$

$$\Delta_7 = \begin{vmatrix} a_1 & a_0 & 0 & 0 & 0 & 0 & 0 \\ a_3 & a_2 & a_1 & a_0 & 0 & 0 & 0 \\ a_5 & a_4 & a_3 & a_2 & a_1 & a_0 & 0 \\ a_7 & a_6 & a_5 & a_4 & a_3 & a_2 & a_1 \\ 0 & a_8 & a_6 & a_7 & a_5 & a_4 & a_3 \\ 0 & 0 & 0 & a_8 & a_7 & a_6 & a_5 \\ 0 & 0 & 0 & 0 & 0 & a_8 & a_7 \end{vmatrix}, \tag{B7}$$

$$\Delta_8 = a_8 \Delta_7, \tag{B8}$$

where $a_{1-8}$ are functions of $\omega_T$ and $\eta$, written below Eq. (8). If all $\Delta$ are positive, the real parts of eight roots of $\lambda$ are all negative. First of all, $\Delta_1 = 4\alpha\eta^3 > 0$, and $\Delta_2 = 4\alpha[(1+5\alpha^2) + (\omega_E + 2\omega_K)\eta]\eta^5 > 0$. In addition, $a_8 = [(1+\beta^2)\omega_T^2 - 4\omega_K(\omega_E + \omega_K)]^2 + 4(\omega_E + 2\omega_K)^2\omega_T^2$. Obviously, $a_8 > 0$. So, from Eq. (B8), $\Delta_7$ and $\Delta_8$ have the same sign. Then, we just need to seek the conditions that $\Delta_{3-7}$ are all positive.

The analytic solutions of $\Delta_{4-6} > 0$ are tanglesome. So, as an example in Fig. 4, we depict the lines of $\Delta_{3-7} = 0$ and shade the areas where $\Delta_{3-7} > 0$ for two typical uniaxial

AFMs. By comparing the panels along each row, it can be observed that when increasing $\omega_T$, $\Delta_7$ first becomes negative at a given $\eta$. Thus, the stability of AFM state is determined by the sign of $\Delta_7$. It should be pointed out that this feature still holds if varying $\beta$. From Eq. (B7), $\Delta_7$ is explicitly factorized as $\Delta_7 = 4096\eta^6/(1+\beta^2)^2\Delta_{7a}\Delta_{7b}\Delta_{7c}$, where $\Delta_{7a} = 4\alpha^4\omega_K(\omega_E+\omega_K) - \alpha^2[(1+\alpha\beta)^2 + 2\eta(\omega_E + 2\omega_K)]\omega_T^2 + \eta^2\omega_T^4$, $\Delta_{7b} = \alpha^4[\eta\omega_E^2 + (1+\alpha^2)(\omega_E+2\omega_K)]^2 + \alpha^2(1+\alpha^2)[(1+\alpha^2)(\alpha-\beta)^2 + 2\beta^2\eta^2\omega_E^2 + 2(1+\alpha^2)\beta^2\eta(\omega_E+2\omega_K)]\omega_T^2 + (1+\alpha^2)^2\beta^4\eta^2\omega_T^4$, $\Delta_{7c} = \{\eta(1+\beta^2)[(1+\beta^2)\omega_T^2 + \omega_E^2] + [(1+\alpha\beta)^2 - (\alpha-\beta)^2](\omega_E+2\omega_K)\}^2 + 4(\alpha-\beta)^2(\omega_E+2\omega_K)[(1+\beta^2)\eta\omega_E^2 + (1+\alpha\beta)^2(\omega_E + 2\omega_K)]$. It is evident that $\Delta_{7b} > 0$ and $\Delta_{7c} > 0$. Then, solving $\Delta_{7a} = 0$ yields

$$\omega_{T\pm}^a = \frac{\alpha}{\sqrt{2}\eta}\sqrt{(1+\alpha\beta)^2 + 2\eta(\omega_E+2\omega_K) \pm \sqrt{\left[(1+\alpha\beta)^2 + 2\eta(\omega_E+2\omega_K)\right]^2 - 16\eta^2\omega_K(\omega_E+\omega_K)}}. \tag{B9}$$

We plot the curves of $\omega_T = \omega_{T\pm}^a$ in rightmost column of Fig. 4, which coincide with the contours of $\Delta_7 = 0$ by numeric calculation. By superposing all the regions that $\Delta_{3-7} > 0$ in Fig. 4, it can be observe that the AFM state becomes unstable when $\omega_T > \omega_{T-}^a$. In Eq. (9), $\omega_{T-}^a$ is replaced by $\omega_T^a$ for simplicity.

## APPENDIX C: STABILITY OF FM STATES

Without SOTs, the FM states $\mathbf{m}_1^0 = \mathbf{m}_2^0 = \xi\mathbf{e}_z$ ($\xi = \pm 1$) certainly are unstable equilibria from the viewpoint of energetics. In the presence of SOTs, they could be stable. Expressing $\mathbf{m}_i$ in terms of a static part and a small amplitude dynamic contribution, we assume

$$\mathbf{m}_i = \xi\mathbf{e}_z + X_i e^{\lambda t}\mathbf{e}_x + Y_i e^{\lambda t}\mathbf{e}_y. \tag{C1}$$

By the same linearization procedure used in Appendix B, we obtain the secular equation, which can factorized into the product of two quartic equations,

$$\begin{aligned}&\left(b_0\lambda^4 + b_1\lambda^3 + b_2\lambda^2 + b_3\lambda + b_4\right)\\ &\times\left(c_0\lambda^4 + c_1\lambda^3 + c_2\lambda^2 + c_3\lambda + c_4\right) = 0,\end{aligned} \tag{C2}$$

where

$$b_0 = \eta^2, \tag{C3}$$

$$b_1 = 2\alpha\eta, \tag{C4}$$

$$b_2 = 1 + \alpha^2 + 4\eta\omega_K + 2\beta\eta\xi\omega_T, \tag{C5}$$

$$b_3 = 4\alpha\omega_K + 2(1+\alpha\beta)\xi\omega_T, \tag{C6}$$

$$b_4 = (\beta\xi\omega_T + 2\omega_K)^2 + \omega_T^2, \tag{C7}$$

$$c_0 = \eta^2, \tag{C8}$$

$$c_1 = 2\alpha\eta, \tag{C9}$$

$$c_2 = 1 + \alpha^2 - 4\eta(\omega_E - \omega_K) + 2\beta\eta\xi\omega_T, \tag{C10}$$

$$c_3 = -4\alpha(\omega_E - \omega_K) + 2(1+\alpha\beta)\xi\omega_T, \tag{C11}$$

$$c_4 = [\beta\xi\omega_T - 2(\omega_E - \omega_K)]^2 + \omega_T^2. \tag{C12}$$

According to the Routh-Hurwitz criterion [76–78], the Hurwitz determinants are calculated as

$$\Delta_1^b = 2\alpha\eta, \tag{C13}$$

$$\Delta_2^b = 2\eta^2(1-\alpha\beta)(\omega_{T1} - \xi\omega_T), \tag{C14}$$

$$\Delta_3^b = 4\eta^2(1+\alpha^2)\left(\omega_{T+}^b - \xi\omega_T\right)\left(\xi\omega_T - \omega_{T-}^b\right) \tag{C15}$$

$$\Delta_4^b = b_4\Delta_3^b, \tag{C16}$$

$$\Delta_1^c = 2\alpha\eta, \tag{C17}$$

$$\Delta_2^c = 2\eta^2(1-\alpha\beta)(\omega_{T2} - \xi\omega_T), \tag{C18}$$

$$\Delta_3^c = 4\eta^2(1+\alpha^2)\left(\omega_{T+}^c - \xi\omega_T\right)\left(\xi\omega_T - \omega_{T-}^c\right) \tag{C19}$$

$$\Delta_4^c = c_4\Delta_3^c, \tag{C20}$$

where

$$\omega_{T1} = \frac{\alpha}{\eta}\frac{1}{1-\alpha\beta}(1+\alpha^2+2\eta\omega_K), \tag{C21}$$

$$\omega_{T2} = \frac{\alpha}{\eta}\frac{1}{1-\alpha\beta}[1+\alpha^2-2\eta(\omega_E-\omega_K)], \tag{C22}$$

$$\omega_{T\pm}^b = \frac{\alpha}{2\eta}[(1+\alpha\beta) \pm \sqrt{(1+\alpha\beta)^2 + 8\eta\omega_K}], \tag{C23}$$

$$\omega_{T\pm}^c = \frac{\alpha}{2\eta}[(1+\alpha\beta) \pm \sqrt{(1+\alpha\beta)^2 - 8\eta(\omega_E-\omega_K)}]. \tag{C24}$$

Next, we try to find the conditions where all the Hurwitz determinants are positive. First, and most obviously, $b_4 > 0$, $c_4 > 0$, $\Delta_1^b > 0$, and $\Delta_1^c > 0$. Then, from Eqs. (C16) and (C20), $\Delta_4^{b,c}$ has the same sign as $\Delta_3^{b,c}$. Hence, we only need to determine the signs of $\Delta_{2,3}^b$ and $\Delta_{2,3}^c$. In view of the strong exchange interaction, it is reasonable to assume that $\omega_E > \omega_K$. Then, if $\eta > \eta_c$ with

$$\eta_c = \frac{(1+\alpha\beta)^2}{8(\omega_E-\omega_K)}, \tag{C25}$$

$\omega_{T\pm}^c$ are conjugate complex. It is easy to infer that $\Delta_3^c < 0$, i.e., the FM states are unstable.

Second, given $\alpha \sim 10^{-2}$, we assume $1 \pm \alpha\beta > 0$ for a moderate estimate of $\beta$. Then, on the promise of $\eta < \eta_c$, the conditions that $\Delta_{1-4}^{b,c} > 0$ are $\xi\omega_T < \omega_{T1}$, $\xi\omega_T < \omega_{T2}$, $\omega_{T-}^b < \xi\omega_T < \omega_{T+}^b$, and $\omega_{T-}^c < \xi\omega_T < \omega_{T+}^c$. Furthermore,

it can be proved that $\omega^c_{T+} < \omega_{T2} < \omega_{T1}$, $\omega^c_{T+} < \omega^b_{T+}$, and $\omega^b_{T-} < \omega^c_{T-}$. Then, the conditions are simplified as $\omega^c_{T-} < \xi\omega_T < \omega^c_{T+}$. For the FM state $\mathbf{m}^0_1 = \mathbf{m}^0_2 = \mathbf{e}_z$, the stable region is $\omega^c_{T-} < \omega_T < \omega^c_{T+}$. While for $\mathbf{m}^0_1 = \mathbf{m}^0_2 = -\mathbf{e}_z$, the stable region is $-\omega^c_{T+} < \omega_T < -\omega^c_{T-}$. This phase boundary is consistent with the boundary of precession state [Eq. (14)].


[1] D. M. Mittleman, Perspective: Terahertz science and technology, J. Appl. Phys. **122**, 230901 (2017).

[2] A. Manchon, J. Železný, I. M. Miron, T. Jungwirth, J. Sinova, A. Thiaville, K. Garello, and P. Gambardella, Current-induced spin-orbit torques in ferromagnetic and antiferromagnetic systems, Rev. Mod. Phys. **91**, 035004 (2019).

[3] I. Firastrau, L. D. Buda-Prejbeanu, B. Dieny, and U. Ebels, Spin-torque nano-oscillator based on a synthetic antiferromagnet free layer and perpendicular to plane polarizer, J. Appl. Phys. **113**, 113908 (2013).

[4] Y. Zhou, J. Xiao, G. E. W. Bauer, and F. C. Zhang, Field-free synthetic-ferromagnet spin torque oscillator, Phys. Rev. B **87**, 020409(R) (2013).

[5] Ø. Johansen and J. Linder, Current driven spin-orbit torque oscillator: Ferromagnetic and antiferromagnetic coupling, Sci. Rep. **6**, 33845 (2016).

[6] H. Zhong, S. Qiao, S. Yan, L. Liang, Y. Zhao, and S. Kang, Terahertz spin-transfer torque oscillator based on a synthetic antiferromagnet, J. Magn. Magn. Mater. **497**, 166070 (2020).

[7] Q. Zhang, Y. Yang, Z. Luo, Y. Xu, R. Nie, X. Zhang, and Y. Wu, Terahertz emission from an exchange-coupled synthetic antiferromagnet, Phys. Rev. Appl. **13**, 044052 (2020).

[8] I. Volvach, A. D. Kent, E. E. Fullerton, and V. Lomakin, Spin-transfer-torque oscillator with an antiferromagnetic exchange-coupled composite free layer, Phys. Rev. Appl. **18**, 024071 (2022).

[9] R. Cheng, M. W. Daniels, J.-G. Zhu, and D. Xiao, Ultrafast switching of antiferromagnets via spin-transfer torque, Phys. Rev. B **91**, 064423 (2015).

[10] R. Cheng, D. Xiao, and A. Brataas, Terahertz antiferromagnetic spin Hall nano-oscillator, Phys. Rev. Lett. **116**, 207603 (2016).

[11] R. Khymyn, I. Lisenkov, V. Tiberkevich, B. A. Ivanov, and A. Slavin, Antiferromagnetic THz-frequency Josephson-like oscillator driven by spin current, Sci. Rep. **7**, 43705 (2017).

[12] R. Zarzuela and Yaroslav Tserkovnyak, Antiferromagnetic textures and dynamics on the surface of a heavy metal, Phys. Rev. B **95**, 180402(R) (2017).

[13] J. Chęciński, M. Frankowski, and T. Stobiecki, Antiferromagnetic nano-oscillator in external magnetic fields, Phys. Rev. B **96**, 174438 (2017).

[14] X. Z. Chen, R. Zarzuela, J. Zhang, C. Song, X. F. Zhou, G. Y. Shi, F. Li, H. A. Zhou, W. J. Jiang, F. Pan, and Y. Tserkovnyak, Antidamping-torque-induced switching in biaxial antiferromagnetic insulators, Phys. Rev. Lett. **120**, 207204 (2018).

[15] P. Stremoukhov, A. Safin, M. Logunov, S. Nikitov, and A. Kirilyuk, Spintronic terahertz-frequency nonlinear emitter based on the canted antiferromagnet-platinum bilayers, J. Appl. Phys. **125**, 223903 (2019).

[16] V. Puliafito, R. Khymyn, M. Carpentieri, B. Azzerboni, V. Tiberkevich, A. Slavin, and G. Finocchio, Micromagnetic modeling of terahertz oscillations in an antiferromagnetic material driven by the spin Hall effect, Phys. Rev. B **99**, 024405 (2019).

[17] R. E. Troncoso, K. Rode, P. Stamenov, J. M. D. Coey, and A. Brataas, Antiferromagnetic single-layer spin-orbit torque oscillators, Phys. Rev. B **99**, 054433 (2019).

[18] D.-K. Lee, B.-G. Park, and K.-J. Lee, Antiferromagnetic oscillators driven by spin currents with arbitrary spin polarization directions, Phys. Rev. Appl. **11**, 054048 (2019).

[19] A. Parthasarathy, E. Cogulu, A. D. Kent, and S. Rakheja, Precessional spin-torque dynamics in biaxial antiferromagnets, Phys. Rev. B **103**, 024450 (2021).

[20] G. Consolo, G. Valenti, A. R. Safin, S. A. Nikitov, V. Tyberkevich, and A. Slavin, Theory of the electric field controlled antiferromagnetic spin Hall oscillator and detector, Phys. Rev. B **103**, 134431 (2021).

[21] B. Wolba, O. Gomonay, and V. P. Kravchuk, Chaotic antiferromagnetic nano-oscillator driven by spin torque, Phys. Rev. B **104**, 024407 (2021).

[22] Q.-H. Li, P.-B. He, M.-Q. Cai, and Z.-D. Li, Equilibria and precession in a uniaxial antiferromagnet driven by the spin Hall effect, New J. Phys. **23**, 113020 (2021).

[23] Y.-Q. Zhao, P.-B. He, and M.-Q. Cai, Tunable range of terahertz oscillations triggered by the spin Hall effect in a biaxial antiferromagnet, Phys. Rev. B **106**, 134427 (2022).

[24] O. R. Sulymenko, O. V. Prokopenko, V. S. Tiberkevich, A. N. Slavin, B. A. Ivanov, and R. S. Khymyn, Terahertz-frequency spin Hall auto-oscillator based on a canted antiferromagnet, Phys. Rev. Appl. **8**, 064007 (2017).

[25] O. V. Gomonay and V. M. Loktev, Using generalized Landau-Lifshitz equations to describe the dynamics of multi-sublattice antiferromagnets induced by spin-polarized current, Low Temp. Phys. **41**, 698 (2015).

[26] G. Gurung, D.-F. Shao, and E. Y. Tsymbal, Spin-torque switching of noncollinear antiferromagnetic antiperovskites, Phys. Rev. B **101**, 140405(R) (2020).

[27] Y. Takeuchi, Y. Yamane, J.-Y. Yoon, R. Itoh, B. Jinnai, S. Kanai, J. Ieda, S. Fukami, and H. Ohno, Chiral-spin rotation of noncollinear antiferromagnet by spin-orbit torque, Nature Mater. **20**, 1364 (2021).

[28] D.-Y. Zhao, P.-B. He, and M.-Q. Cai, Terahertz oscillation in a noncollinear antiferromagnet under spin-orbit torques, Phys. Rev. B **104**, 214423 (2021).

[29] A. Shukla and S. Rakheja, Spin-torque-driven terahertz auto-oscillations in noncollinear coplanar antiferromagnets, Phys. Rev. Appl. **17**, 034037 (2022).

[30] I. Lisenkov, R. Khymyn, J. Åkerman, N. X. Sun, and B. A. Ivanov, Subterahertz ferrimagnetic spin-transfer torque oscillator, Phys. Rev. B **100**, 100409(R) (2019).

[31] F. Cutugno, L. Sanchez-Tejerina, R. Tomasello, M. Carpentieri, and G. Finocchio, Micromagnetic understanding of switching and self-oscillations in ferrimagnetic materials, Appl. Phys. Lett. **118**, 052403 (2021).

[32] M. Guo, H. Zhang, and R. Cheng, Manipulating ferrimagnets by fields and currents, Phys. Rev. B **105**, 064410 (2022).

[33] R. Mondal, L. Rózsa, M. Farle, P. M. Oppeneer, U. Nowak, and M. Cherkasskii, Inertial effects in ultrafast spin dynamics, J. Magn. Magn. Mater. **579**, 170830 (2023).

[34] T. L. Gilbert, A phenomenological theory of damping in ferromagnetic materials, IEEE Trans. Magn. **40**, 3443 (2004).

[35] M.-C. Ciornei, J. M. Rubí, and J.-E. Wegrowe, Magnetization dynamics in the inertial regime: Nutation predicted at short time scales, Phys. Rev. B **83**, 020410(R) (2011).

[36] J.-E. Wegrowe and M.-C. Ciornei, Magnetization dynamics, gyromagnetic relation, and inertial effects, Am. J. Phys. **80**, 607 (2012).

[37] S. Giordano and P.-M. Déjardin, Magnetization dynamics, gyromagnetic relation, and inertial effects, Phys. Rev. B **102**, 214406 (2020).

[38] M. Fähnle, D. Steiauf, C. Illg, Generalized Gilbert equation including inertial damping: Derivation from an extended breathing Fermi surface model, Phys. Rev. B **84**, 172403 (2011).

[39] M. Fähnle and C. Illg, Electron theory of fast and ultrafast dissipative magnetization dynamics, J. Phys.: Condens. Matter **23**, 493201 (2011).

[40] R. Mondal, M. Berritta, A. K. Nandy, and P. M. Oppeneer, Relativistic theory of magnetic inertia in ultrafast spin dynamics, Phys. Rev. B **96**, 024425 (2017).

[41] R. Mondal, M. Berritta, and P. M. Oppeneer, Generalisation of Gilbert damping and magnetic inertia parameter as a series of higher-order relativistic terms, J. Phys.: Condens. Matter **30**, 265801 (2018).

[42] U. Bajpai and B. K. Nikolić, Time-retarded damping and magnetic inertia in the Landau-Lifshitz-Gilbert equation self-consistently coupled to electronic time-dependent nonequilibrium Green functions, Phys. Rev. B **99**, 134409 (2019).

[43] S. Bhattacharjee, L. Nordström, and J. Fransson, Atomistic spin dynamic method with both damping and moment of inertia effects included from first principles, Phys. Rev. Lett. **108**, 057204 (2012).

[44] P. Thibaudeau and S. Nicolis, Emerging magnetic nutation, Eur. Phys. J. B **94**, 196 (2021).

[45] Y. Li, A.-L. Barra, S. Auffret, U. Ebels, and W. E. Bailey, Inertial terms to magnetization dynamics in ferromagnetic thin films, Phys. Rev. B **92**, 140413(R) (2015).

[46] K. Neeraj, N. Awari, S. Kovalev, D. Polley, N. Z. Hagström, S. S. P. K. Arekapudi, A. Semisalova, K. Lenz, B. Green, J.-C. Deinert, I. Ilyakov, M. Chen, M. Bawatna, V. Scalera, M. d¡¯Aquino, C. Serpico, O. Hellwig, J.-E. Wegrowe, M. Gensch, and S. Bonetti, Inertial spin dynamics in ferromagnets, Nature Phys. **17**, 245 (2021).

[47] V. Unikandanunni, R. Medapalli, M. Asa, E. Albisetti, D. Petti, R. Bertacco, E. E. Fullerton, and S. Bonetti, Inertial spin dynamics in epitaxial cobalt films, Phys. Rev. Lett. **129**, 237201 (2022).

[48] E. Olive, Y. Lansac, and J.-E. Wegrowe, Beyond ferromagnetic resonance: The inertial regime of the magnetization, Appl. Phys. Lett. **100**, 192407 (2012).

[49] D. Böttcher and J. Henk, Significance of nutation in magnetization dynamics of nanostructures, Phys. Rev. B **86**, 020404(R) (2012).

[50] E. Olive, Y. Lansac, M. Meyer, M. Hayoun, and J.-E. Wegrowe, Deviation from the Landau-Lifshitz-Gilbert equation in the inertial regime of the magnetization, J. Appl. Phys. **117**, 213904 (2015).

[51] M. Cherkasskii, M. Farle, and A. Semisalova, Deterministic inertial dynamics of the magnetization of nanoscale ferromagnets, Phys. Rev. B **102**, 184432 (2020).

[52] R. Mondal, Theroy of magnetic inertial dynamics in two-sublattice ferromagnets, J. Phys.: Condens. Matter **33**, 275804 (2021).

[53] S. V. Titov, W. T. Coffey, Y. P. Kalmykov, and M. Zarifakis, Deterministic inertial dynamics of the magnetization of nanoscale ferromagnets, Phys. Rev. B **103**, 214444 (2021).

[54] M. Cherkasskii, I. Barsukov, R. Mondal, M. Farle, and A. Semisalova, Theory of inertial spin dynamics in anisotropic ferromagnets, Phys. Rev. B **106**, 054428 (2022).

[55] S. V. Titov, W. J. Dowling, and Y. P. Kalmykov, Ferromagnetic and nutation resonance frequencies of nanomagnets with various magnetocrystalline anisotropies, J. Appl. Phys. **131**, 193901 (2022).

[56] R. Mondal, S. Großenbach, L. Rózsa, and U. Nowak, Nutation in antiferromagnetic resonance, Phys. Rev. B **103**, 104404 (2021).

[57] R. Mondal and P. M. Oppeneer, Influence of intersublattice coupling on the terahertz nutation spin dynamics in antiferromagnets, Phys. Rev. B **104**, 104405 (2021).

[58] R. Mondal and A. Kamra, Spin pumping at terahertz nutation resonances, Phys. Rev. B **104**, 214426 (2021).

[59] I. Makhfudz, E. Olive, and S. Nicolis, Nutation wave as a platform for ultrafast spin dynamics in ferromagnets, Appl. Phys. Lett. **117**, 132403 (2020).

[60] M. Cherkasskii, M. Farle, and A. Semisalova, Dispersion relation of nutation surface spin waves in ferromagnets, Phys. Rev. B **103**, 174435 (2021).

[61] A. M. Lomonosov, V. V. Temnov, and J.-E. Wegrowe, Nutation spin waves in ferromagnets, Phys. Rev. B **104**, 054425 (2021).

[62] S. V. Titov, W. J. Dowling, Y. P. Kalmykov, and M. Cherkasskii, Nutation spin waves in ferromagnets, Phys. Rev. B **105**, 214414 (2022).

[63] R. Mondal and L. Rózsa, Inertial spin waves in ferromagnets and antiferromagnets, Phys. Rev. B **106**, 134422 (2022).

[64] R. Rahman and S. Bandyopadhyay, An observable effect of spin inertia in slow magneto-dynamics: Increase of the switching error rates in nanoscale ferromagnets, J. Phys.: Condens. Matter **33**, 355801 (2021).

[65] K. Neeraj, M. Pancaldi, V. Scalera, S. Perna, M. d'Aquino, C. Serpico, and S. Bonetti, Magnetization switching in the inertial regime, Phys. Rev. B **105**, 054415 (2022).

[66] I. Makhfudz, Y. Hajati, and E. Olive, High-temperature magnetization reversal in the inertial regime, Phys. Rev. B **106**, 134415 (2022).

[67] L. Winter, S. Großenbach, U. Nowak, and L. Rózsa, Nutational switching in ferromagnets and antiferromagnets, Phys. Rev. B **106**, 214403 (2022).

[68] G. Bertotti, C. Serpico, I. D. Mayergoyz, A. Magni, M. dAquino, and R. Bonin, Magnetization switching and microwave oscillations in nanomagnets driven by spin-polarized currents, Phys. Rev. Lett. **94**, 127206 (2005).

[69] T. Taniguchi, Nonlinear analysis of magnetization dynamics excited by spin Hall effect, Phys. Rev. B **91**, 104406 (2015).

[70] D. Thonig, O. Eriksson, and M. Pereiro, Magnetic moment of inertia within the torque-torque correlation model, Sci. Rep. **7**, 931 (2017).

[71] Lijun Zhu, D. C. Ralph, and R. A. Buhrman, Highly efficient spin-current generation by the spin Hall effect in $Au_{1-x}Pt_x$, Phys. Rev. Appl. **10**, 031001(R) (2018).

[72] C. F. Pai, Y. Ou, L. H. Vilela-Leão, D. C. Ralph, and R. A. Buhrman, Dependence of the efficiency of spin Hall torque on the transparency of Pt/ferromagnetic layer interfaces, Phys. Rev. B **92**, 064426 (2015).

[73] Z. L. Wang, H. Y. Cheng, K. W. Shi, Y. Liu, J. F. Qiao, D. Q. Zhu, W. L. Cai, X. Y. Zhang, S. Eimer, D. P. Zhu, J. Zhang, A. Fert, and W. S. Zhao, Modulation of field-like spin orbit torque in heavy metal/ferromagnet heterostructures, Nanoscale **12**, 15246 (2020).

[74] S. M. Rezende, A. Azevedo, and R. L. Rodríguez-Suárez, Introduction to antiferromagnetic magnons, J. Appl. Phys. **126**, 151101 (2019).

[75] R. C. Ohlmann and M. Tinkham, Antiferromagnetic resonance in $FeF_2$ at far-infrared frequencies, Phys. Rev. **123**, 425 (1961).

[76] F. R. Gantmacher, *Applications of the Theory of Matrices* (Wiley, New York, 1959), p. 231.

[77] L. J. S. Allen, *An Introduction to Mathematical Biology* (Pearson Education, London, 2007), p. 150.

[78] P. Baláž and J. Barnaś, Current-induced instability of a composite free layer with antiferromagnetic interlayer coupling, Phys. Rev. B **88**, 014406 (2013).

[79] P. Vaidya, S. A. Morley, J. V. Tol, Y. Liu, R. Cheng, A. Brataas, D. Lederman, and E. D. Barco, Subterahertz spin pumping from an insulating antiferromagnet, Science **368**, 160 (2020).

[80] S. Blundell, *Magnetism in Condensed Matter*, (Oxford University Press, Oxford, 2001), pp. 94–96.

[81] F. L. A. Machado, P. R. T. Ribeiro, J. Holanda, R. L. Rodríguez-Suárez, A. Azevedo, and S. M. Rezende, Spin-flop transition in the easy-plane antiferromagnet nickel oxide, Phys. Rev. B **95**, 104418 (2017).

[82] T. Hirai, K. Hasegawa, S. Ota, M. Suzuki, T. Koyama, and D. Chiba, Modification of interfacial spin-orbit torque in Co/Pt/oxide hybrid structures, Phys. Rev. B **104**, 134401 (2021).

[83] L. Chen, K. Zollner, S. Parzefall, J. Schmitt, M. Kronseder, J. Fabian, D. Weiss, and C. H. Back, Connections between spin-orbit torques and unidirectional magnetoresistance in ferromagnetic-metal-heavy-metal heterostructures, Phys. Rev. B **105**, L020406 (2022).